EXPEDITED PUBLICATION

Magnetic Resonance Spectroscopy Guided Brain Tumor Resection: Differentiation Between Recurrent Glioma and Radiation Change in Two Diagnostically Difficult Cases

Mark C. Preul, Richard Leblanc, Zografos Caramanos, Reza Kasrai, Sridar Narayanan and Douglas L. Arnold

ABSTRACT: ***Background:*** It is often difficult to differentiate a recurrent glioma from the effects of post-operative radiotherapy by means of conventional neurodiagnostic imaging. Proton magnetic resonance spectroscopic imaging (^{1}H-MRSI), that allows *in vivo* measurements of the concentration of brain metabolites such as choline-containing phospholipids (Cho), may provide *in vivo* biochemical information helpful in distinguishing areas of tumor recurrence from areas of radiation effect. ***Patients and Methods:*** Two patients who had undergone resection and post-operative radiotherapy for a cerebral glioma became newly symptomatic. Computed tomographic (CT) and magnetic resonance imaging (MRI) performed after the intravenous infusion of contrast material, and in one case, [18F]fluorodeoxyglucose positron emission tomography (PET), could not differentiate between the possibilities of recurrent glioma and radiation effect. The patients underwent ^{1}H-MRSI prior to reoperation and the ^{1}H-MRSI results were compared to histological findings originating from the same locations. ***Results:*** A high Cho signal measured by ^{1}H-MRSI was seen in areas of histologically-proven dense tumor recurrence, while low Cho signal was present where radiation changes predominated. ***Conclusions:*** The differentiation between the recurrence of a cerebral glioma and the effects of post-operative irradiation was achieved using ^{1}H-MRSI in these two patients whose conventional neurodiagnostic imaging was equivocal for such a distinction. Where these two conditions are present, metabolite images from ^{1}H-MRSI, such as that based on Cho, can be co-registered with other imaging modalities such as MRI and may also be integrated with functional MRI or functional PET within a multimodal imaging-guided surgical navigation system to assure maximal resection of recurrent tumor while minimizing the risk of added neurological damage.

RÉSUMÉ: Résection d'une tumeur cérébrale sous guidage par spectroscopic de résonance magnetique du proton: distinction entre un gliome récidivant et des changements induits par la radiothérapie. ***Introduction:*** Il est souvent difficile de distinguer par l'imagerie neurodiagnostique conventionnelle entre une récidive d'un gliome et les effets de la radiothérapie postopératoire. L'imagerie par spectroscopie de résonance magnétique du proton (^{1}H-SRM) qui permet de faire des mesures *in vivo* de la concentration de métabolites au niveau du cerveau tels les phospholipides contenant de la choline (Cho), peut fournir des informations biochimiques *in vivo* qui aident à distinguer les zones de récurrence tumorale des zones affectées par la radiothérapie. ***Patients et méthodes:*** Deux patients qui avaient subi une résection d'un gliome cérébral et de la radiothérapie postopératoire ont présenté une récidive de la symptomatologie. La tomodensitométrie et la résonance magnétique après injection intraveinineuse d'une substance de contraste et, dans un cas, la tomographie par émission de position au [18F]fluorodésoxyglucose, n'ont distinguer entre la possibilité d'une récurrence d'un gliome et les effets de la radiothérapie. Les patients ont subi une ^{1}H-SRM avant la réintervention et les résultats de la ^{1}H-SRM ont été comparés aux données histologiques des mêmes sites. ***Résultats:*** Un signal Cho élevé mesuré par ^{1}H-SRM a été observé dans les zones de récurrence tumorale dense avec preuve histologique, alors qu'un signal Cho faible était présent dans les zones où les changements dus à la radiothérapie prédominaient. ***Conclusions:*** La distiction entre la récurrence d'un gliome cérébral et les effets de l'irradiation postopératoire a été faite au moyen de la ^{1}H-SRM chez ces deux patients dont l'imagerie neurodiagnostique conventionnelle était équivoque sur ce paoint. Quand ces deux conditions sont présentes, les images obtenues au moyen de métabolites par la ^{1}H-SRM, dont celles obtenues au moyen de la Cho, peuvent être combinées à d'autres modalités d'imagerie telle la RMN et peuvent également être intégrées à la RMN fonctionnelle ou PET fonctionnel au sein d'un système multimodal de navigation chirurgical guidé par imagerie pour s'assurer d'une résection maximale lorsqu'il y a récurrence tumorale tout en minimisant le risque de dommage neurologigue surajouté.

Can. J. Neurol. Sci. 1998; 25: 13-22

The differentiation of recurrent tumor from radiation necrosis is a commonly encountered problem in patients with a glioma that has been treated with post-operative radiotherapy and is difficult to achieve with conventional neurodiagnostic imaging. Spectra of major brain metabolites based on *in vivo* proton magnetic resonance spectroscopic imaging (^{1}H-MRSI) have been

From the Department of Neurology and Neurosurgery, MR Spectroscopy Unit and NeuroImaging Laboratory, Montreal Neurological Hospital and Institute, Montreal.
RECEIVED NOVEMBER 27, 1997. ACCEPTED IN FINAL FORM JANUARY 6, 1998.
Reprint requests to: Richard Leblanc, Montreal Neurological Institute and Hospital, 3801 University Street, Montreal, Quebec, Canada H3A 2B4

shown to accurately predict the histological nature of the most common types of brain neoplasms.[1,2] Our work in progress correlating regional tumor tissue samples with corresponding ^{1}H-MRSI voxels suggests that the histological features of hypercellularity with and without pleomorphism and necrosis have identifiable ^{1}H-MRSI spectral patterns and that a high concentration of choline-containing phospholipids (Cho) accompanies dense areas of cellular proliferation.[3,4] It has been suggested that the magnitude of the Cho resonance may be reliable in detecting areas of recurrent tumor growth.[5-7] However, histological confirmation of this supposition has heretofore been lacking. We describe two patients with a recurrent glioma that was initially treated with resection and post-operative radiotherapy in whom the concentration of the Cho metabolite differentiated between regions of histologically verified tumor recurrence and areas of radiation effect. The differentiation of recurrent glioma from radiation effect is of obvious importance in the assessment and treatment of patients with a recurrent glioma.

Patients and Methods

Patient 1 – Clinical History

A 39-year-old white male developed focal motor seizures 18 months prior to admission to our hospital. A computed tomography (CT) scan performed at the time was reported as normal. A recurrence of seizures 12 months later prompted reinvestigation and an infused CT scan demonstrated a right frontal, enhancing lesion and associated edema. This lesion was resected and histological examination revealed a glioblastoma multiforme. The patient underwent post-operative radiotherapy, with 2 opposing fields covering the cranium, receiving 40 Gy in 20 treatments and the fields thereafter decreased for a total of 60 Gy in 30 treatments.

Six months after his initial surgery, an infused CT scan suggested tumor recurrence and the patient was referred for surgery involving a gene therapy protocol using a herpes simplex virus-thymidine kinase gene/ganciclovir system as approved by the Investigational Review Board of McGill University.[8-12] The patient underwent MRI with and without gadolinium that suggested radiation necrosis or tumor recurrence but could not conclusively differentiate between the two possibilities (Figure 1A). Functional PET scanning demonstrated that the posterior aspect of the gadolinium-enhancing area resided within the motor strip (Figure 2). A non-quantitative FDG PET study was unable to differentiate tumor recurrence from radiation effect as it revealed radioactivity within the whole of the gadolinium-enhancing area on the MRI, moreso posteriorly.

Because of the difficulty in diagnostic interpretation of the above imaging and to optimize surgical planning, the patient had ^{1}H-MRSI in the belief that the area of recurrent tumor could be better identified relative to the imaging evidence from f-PET and to establish if the area of recurrence comprised the entire gadolinium-enhanced area. The anterior part of the gadolinium-enhancing region revealed ^{1}H-MRSI spectra (Figure 1B) showing high Cho and LA which was suspected to harbor tumor recurrence. The ^{1}H-MRSI spectra of the posterior aspect of the gadolinium-enhancing region, including that part extending into the motor strip as demonstrated by f-PET, was interpreted as not harboring viable tumor as reflected by decreased Cho and Cr, and markedly low NA, and high LA. The ^{1}H-MRSI spectra from tissue in the contralateral hemisphere showed a normal metabolic pattern. Cortical mapping under local anesthesia confirmed the relationship of the abnormal tissue to the motor strip as demonstrated by f-PET.

Using the ^{1}H-MRSI-MRI, resection was confined mainly to the area of high Cho signal, histological examination of which confirmed recurrent glioblastoma multiforme (Figure 3A and B). Biopsies into the area posterior to the high Cho signal and which enhanced with gadolinium on MRI, confirmed the presence of radiation necrosis. Multimodal image integration (Figure 4) confirmed the relationship of the area of high Cho signal to the motor strip, as defined by f-PET, and to the area of gadolinium enhancement, as observed intraoperatively.

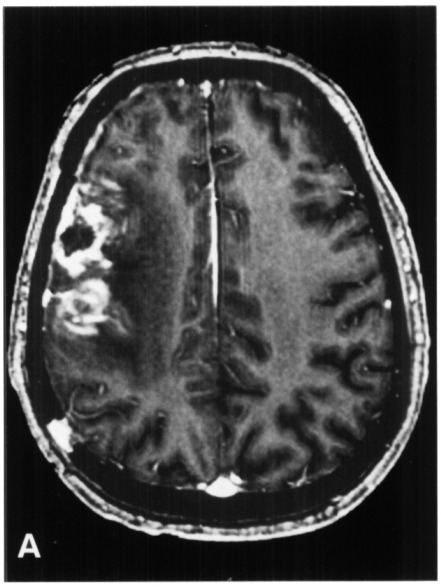

Figure 1: A) *Gadolinium-enhanced MRI demonstrating a large area of enhancement in the right frontal lobe six months after initial surgery and post-operative radiotherapy.*

The patient awoke from surgery, which included instillation of the herpes simplex-thymidine kinase gene vector solution into the resection margins according to protocol, without new neurological deficits. After a stable course of approximately one year, the patient died of pneumonia. Post mortem examination of the brain revealed that most of the area corresponding to the gadolinium enhancement was radiation necrosis. Viable tumor cells were found in the margins of the resection cavity, i.e., in the area of high Cho signal. Tumor was not found in the posterior area which had shown high activity on FDG PET.

Patient 2 – Clinical History

A 44-year-old male with a history of a resection of a right frontal grade II oligodendroglioma 2 years previously, followed by post-operative radiation therapy to the right frontal area (54 Gy in 30 treatments) was admitted to hospital with worsening memory and a left hemiparesis of 3 months duration. A CT scan following injection of intravenous contrast material showed the area of previous resection although there was no enhancement and minimal mass effect. There were no areas of hypo- or hyperdensity. MRI showed only mild hyperintense signal on T_2-weighted images posterior and lateral to the area of previous resection, raising the suspicion of tumor recurrence. There was no enhancement with gadolinium. Because of the minimal signal changes, no enhancement, and lack of clear mass effect, neurologic deterioration due to radiation effect was also considered.

The patient underwent ^{1}H-MRSI in the hopes that it would more clearly define the area(s) of tumor recurrence and optimize surgical planning. The Cho image showed areas of high signal intensity anterior and posterior to the previous resection which were suspected to be areas of tumor recurrence (Figure 5A). The image based on the NA resonance showed decreased signal intensity in these same areas indicating loss of neurons. There were no areas of high Cho signal intensity lateral to the previous resection cavity.

As predicted by ^{1}H-MRSI, the histological examination of the tissue obtained at reoperation confirmed the presence of recurrent tumor in the anterior and posterior aspects of the previous resection cavity in areas that had shown a Cho signal of high intensity: recurrent grade II oligodendroglioma was found anteriorly and recurrent oligodendroglioma (Figure 5B) with malignant features posteriorly. The proximity of the posterior high Cho signal area to the motor strip permitted biopsy only, while a more extensive resection was carried out anteriorly. Histological examination from biopsies into the area lateral to the previous resection cavity that had exhibited low Cho signal demonstrated predominantly radiation changes without necrosis (Figure 5C).

https://doi.org/10.1017/S0317167100033436 Published online by Cambridge University Press

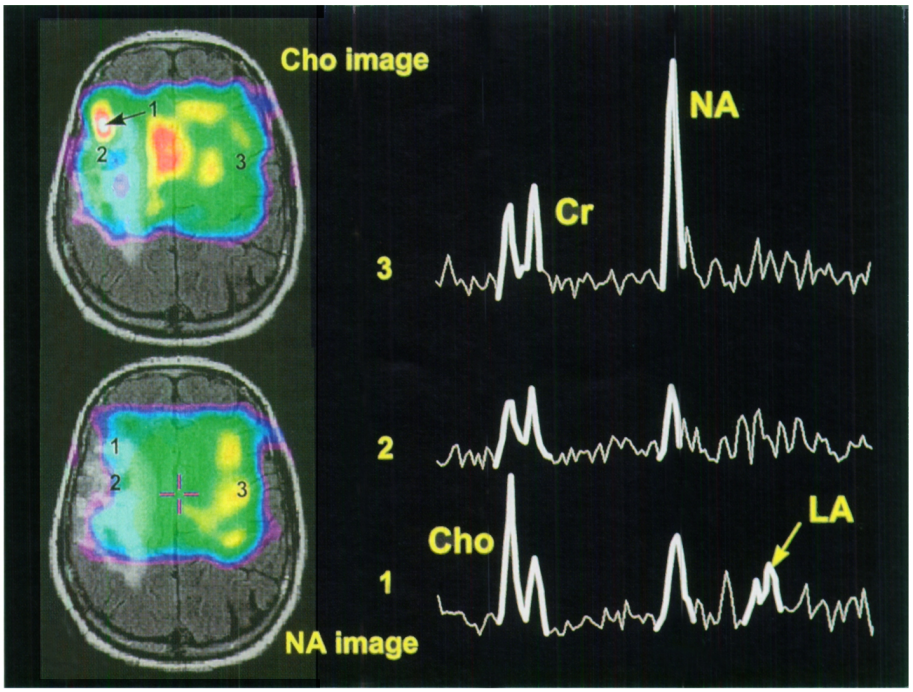

Figure 1: *B) Co-registered ^{1}H-MRSI-MRI images are shown for choline (Cho) (top) and N-acetylaspartate (NA) (bottom). Three numbered spectra originate from 1 ml voxels in numbered locations on the images. Note the high Cho in area 1 on the Cho image and in spectrum 1 reflecting an area of histologically verified recurrent tumor. Spectrum 1 also shows the lactate (LA) found in this area. Note also the moderately decreased Cho and Cr and markedly decreased NA (see NA image) in spectrum 2 correlating with radiation changes. Spectrum 3 shows a normal biochemical pattern from a contralateral voxel. (The relevant main metabolite peaks have been bolded for clarity.)*

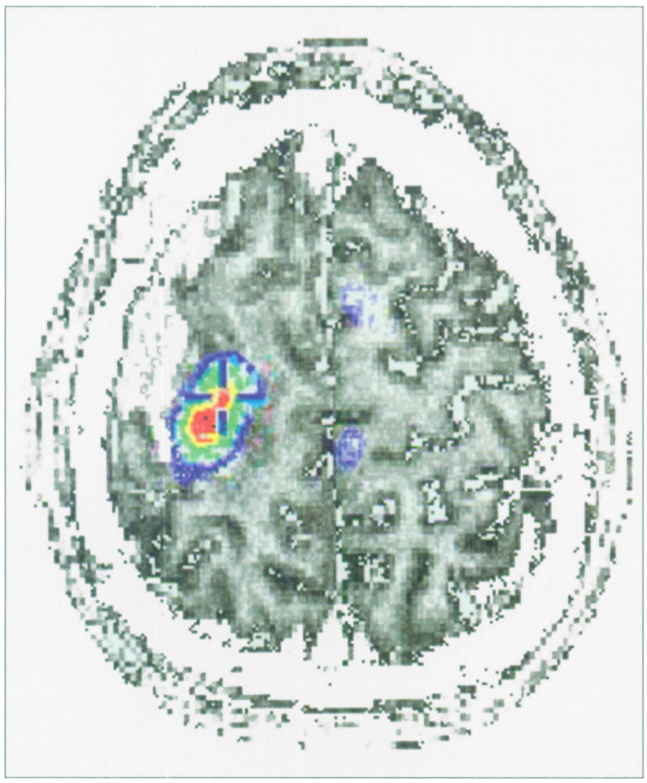

Figure 2: *Functional PET scan obtained during performance of a motor-hand task demonstrating the relationship of the area of gadolinium enhancement to the motor strip.*

The patient awoke without new neurologic deficits, and was clinically stable for approximately 2 months after surgery. He did not return for follow-up, but was reported to have clinically deteriorated and died, presumably from progression of the posterior portion of recurrent tumor that could not be resected.

^{1}H-MRSI Methods and Image Integration

Conventional MR scans, as well as two-dimensional ^{1}H-MRSI scans, were acquired using a 1.5 Tesla imaging/spectroscopy system (Gyroscan ACS II/III Philips Medical Systems, Best, The Netherlands). The acquired data can be displayed either as a multitude of chemical spectra from voxels (small tissue volumes) within a larger region of interest (ROI) or in tomographic format, i.e., maps based on individual or multiple chemical peaks which display the regional heterogeneous distribution of metabolites within the ROI.[2,13-16] A large region of interest (ROI) which included the tumor, as well as either contralateral or remote normal-appearing brain tissue, was defined for selective excitation. Regions of interest ranged in size from 100-120 mm antero-posterior, 100-120 mm medial-lateral, and 15-20 mm cranio-caudal. These were aligned parallel to the transverse MRI scout slices and spectra were obtained using a 90°-180°-180° (PRESS) pulse sequence for volume selection. Water was suppressed by selective excitation. The following acquisition parameters were used: an inter-pulse delay (TR) of 2000 ms; a spin-echo refocusing time (TE) of 272 ms; a field of view (FOV) of 250 x 250 mm^2; 32 x 32 phase encoding steps; and 1 signal average per phase-encoding step. The water-suppressed was followed by a non-water-suppressed image obtained using a TR of 850 ms, a TE of 272 ms, a FOV of 250 x 250 mm^2 and 16 x 16 phase encoding steps. To correct for

https://doi.org/10.1017/S0317167100033436 Published online by Cambridge University Press

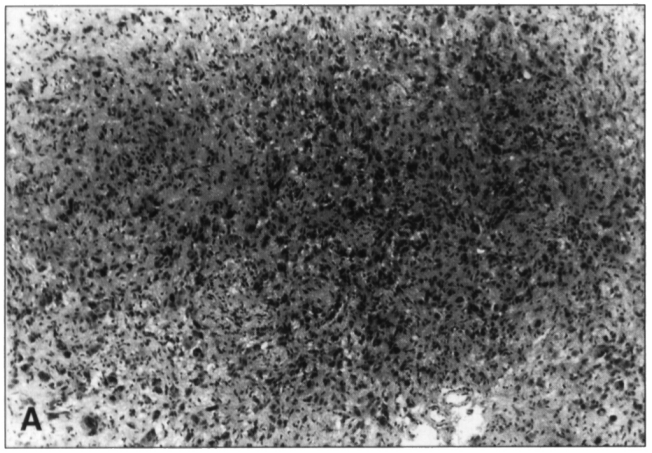

Figure 3: A) *Histopathology of the tissue from voxel 1 as labeled on Figure 1 which showed increased Cho and LA, revealing a mass of bizarre, gemistocytic-like, markedly pleomorphic astrocytes consistent with a malignant glioma.*

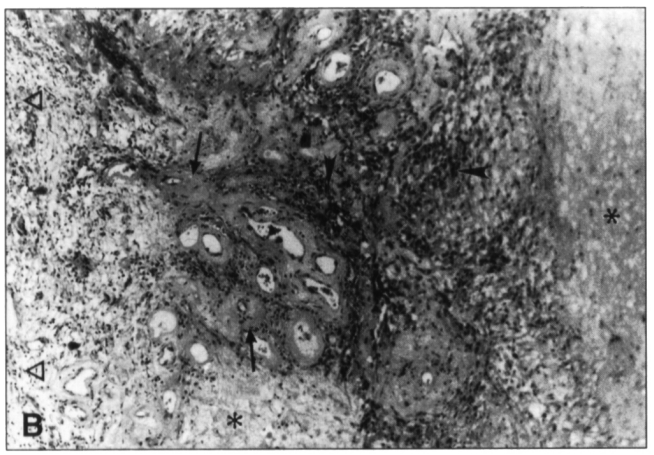

Figure 3: B) *Histopathology of tissue originating from the area of voxel 2 as labeled on Figure 1, which showed less Cho and LA, revealing extensive radiation changes characterized by thickened vessel walls (arrows), reactive astrocytosis (areas marked by triangles), macrophage infiltration (arrowheads), and areas of necrosis (areas marked by asterisks). (Hematoxylin and eosin, 100 X)*

artifacts arising from magnetic field inhomogeneities, the water-suppressed ^{1}H-MRSI was divided by the unsuppressed ^{1}H-MRSI after zero-filling the latter to 32 x 32 profiles. This yielded a nominal voxel (tissue volume) size of 0.7 to 1.0 ml (depending on ROI thickness). Total imaging time, including ROI definition, shimming, gradient tuning, and ^{1}H-MRSI acquisition ranged from 55 min to 85 min; acquisition of the ^{1}H-MRSI itself taking 41 minutes.

Post-processing of data and ^{1}H-MRSI image creation was performed using XUNSPEC1 software (Philips Medical Systems, Best, The Netherlands) running on a Sun SPARC workstation (Sun Microsystems Computer Corp., Mountain View, CA). This included a mild Gaussian filter and an inverse two-dimensional Fourier transform to both the water-suppressed and -unsuppressed ^{1}H-MRSI. Water was further suppressed by left shifting the time domain data and subtracting it from itself. This procedure modulates the amplitude of the spectrum and increases the ratio of NA/Cr, but by an amount that is proportional to the true NA/Cr ratio in each voxel.

Resonance intensity measurements (expressed in volts per hertz) were obtained for five of the major chemical resonances observed in the T_2-weighted ^{1}H-MRSI spectrum of gliomas *in vivo*. Expressed as the difference in parts per million (ppm) between the resonance frequency of the compound of interest and that of tetramethylsilane, these five resonances included: (1) Cho at 3.2 ppm; (2) Cr at 3.0 ppm; (3) NA at 2.0 ppm; (4) LA at 1.3 ppm; and (5) Lip between 1.3 and 0.9 ppm. Automated calculation of metabolite peak areas was performed on operator-selected voxels within the ^{1}H-MRSI ROIs. For each selected voxel, ranges of the selected metabolite peaks (i.e., Cho, Cr, NA, LA, Lip) were delineated by searching for local minima which straddle a local maximum in predefined ranges of the MR spectrum. Peaks were digitally integrated to yield areas. Peak intensities were normalized by dividing them by the peak intensity of Cr[17] in MRI-normal-appearing voxels located in the contralateral, homologous area. If that was not possible, they were normalized to Cr values in voxels located in remote, MRI-normal-appearing brain tissue.

Metabolite images were reconstructed (XUNSPEC1 software [Philips Medical Systems, Best, The Netherlands]) from the major peaks in the proton spectra showing the regional distribution of choline-containing phospholipids (Cho - 3.2 ppm); creatine and phosphocreatine (Cr - 3.0 ppm), important for cellular energy status; N-acetyl-containing compounds (NA - 2.0 ppm), the dominant contribution being from N-acetylaspartate, a neuronal marker; and lactate (LA - 1.3 ppm), an indirect marker of abnormal glycolysis. For purposes of image correlation and surgical guidance, the ^{1}H-MRSI metabolite images and transverse MRI were resampled to the same voxel size and co-registered. If necessary, (as in our second patient) a combined imaging data set using the metabolite images integrated with a global MRI data set, could be merged, along with other imaging modalities, e.g., f-PET or FDG PET images, into an interactive, image-guided planning system that allowed for frameless stereotactic surgical navigation.

Among the metabolite images, particular attention was paid to the Cho image to identify and navigate during surgery to areas of suspected tumor recurrence and radiation change based upon the high or low Cho signal, respectively, in the corresponding area. The elevated Cho signal probably reflects an increase in metabolites that are precursors of the membrane phospholipids involved in neoplastic proliferation. [2,13-16,18]

Co-registration of ^{1}H-MRSI and MRI

The process of registering ^{1}H-MRSI images and anatomical MRI images required two sets of acquisitions. Before the acquisition of any MR spectra, a targeting MR volume (or "slab") was acquired in order to localize the volume of interest for subsequent ^{1}H-MRSI acquisitions. A variety of MR imaging sequences can be used for this initial volume depending on the desired image contrast. However, since the image contrast of this slab influences the accuracy of the registration process it is preferable to use a T_1-weighted sequence (as in our first patient) which enhances skin features. MR spectra were acquired immediately after the localization process, and we assumed that these two sets of images (the ^{1}H-MRSI and the targeting MRI) are already registered. This approximation is valid assuming no

https://doi.org/10.1017/S0317167100033436 Published online by Cambridge University Press

patient movement between the scans. The patients' heads were placed into a special cushioned headrest which immobilizes the head. The metabolite maps (^{1}H-MRSI images) are generated from the MR spectra and they are typically linearly interpolated onto a 256 x 256 x 15 mm^3 "slab".

Integrating ^{1}H-MRSI Into an Image-guided, Frameless Stereotactic System

For integration with the interactive, frameless stereotactic guidance system (Viewing Wand, ISG Technologies, Inc., Toronto, Canada and the Visual Integration Platform for Enhanced Reality [VIPER], NeuroImaging Laboratory, Montreal Neurological Institute, McGill University, Montreal, Canada), a third image set was acquired: a standard T_1-weighted high-resolution (1 mm^3) 3-D gradient-echo global volume of the head. The ^{1}H-MRSI was then registered to the global MRI. Since the ^{1}H-MRSI lack detailed structural information, the targeting volume acquired immediately prior to the ^{1}H-MRSI acquisition was used to calculate a transformation between the ^{1}H-MRSI-space and the global MRI-space. The targeting MRI acquired before the spectra is used to obtain the transformation, since it has enough structural information to allow the matching of corresponding features between the two volumes. The same transformation was then used to resample the ^{1}H-MRSI into the global MRI space. This registration procedure can be performed in two ways. If the targeting volume is such that a sufficient number of landmarks can be identified which exist in both MR volumes, a point-by-point registration may be performed. This involves identifying corresponding (or homologous) points in both volumes and performing a linear least-squares minimization (Procrustes)[19] to obtain a mapping from one space to another. If the targeting volume lacked either the resolution or the contrast for such an operation, we used an automatic linear registration algorithm which requires no manual user intervention. For intrasubject registrations within a modality (i.e., MRI to MRI) an algorithm based on information theory[20] was typically used, although a multi-scale 3-D cross-correlation technique[21] can also be used to align the two volumes into the same space. The result obtained from any of these processes is an affine transformation which maps points in the MRS-space into the global MRI-space. Whereas the results from the latter techniques are user-independent and more reproducible, the point-by-point matching is generally computationally less expensive.

Once a transformation existed between the ^{1}H-MRSI images and the global MRI volume, the metabolite map slabs were resampled into the global MRI-space for each metabolite of interest. The visualization software is flexible such that the multiple data sets are not required to have the same sampling, the same resolution, or the same extent.

After resampling the ^{1}H-MRSI images into the global MRI volume, we rendered corresponding slices from each volume and superimposed them on the computer screen. Each volume was assigned its own opacity value (0 for completely transparent, and 1 for completely opaque), such that the relative blending between all the images could independently and interactively varied. Apart from metabolite images, other functional data sets were also available, e.g., FDG PET, f-PET, or f-MRI studies. The procedure used to register the PET volumes to the global MRI incorporated a ratio of variances minimization algorithm (AIR – Automatic Image Registration).[22]

The merged volumes (MRI, ^{1}H-MRSI, and PET) were visualized using a standard tri-planar display, where the intersection of the three orthogonal cuts (sagittal, coronal, and axial) defined the point of interest (Figure 4). The user could navigate through the volumes using mouse clicks or use keyboard inputs to browse slice by slice.

Considerations of Accuracy and Precision Using ^{1}H-MRSI Integration

The different registration procedures used here have varying results in terms of accuracy and precision. These results are dependent on the modalities involved and the specific method or algorithm employed in the registration. The registration accuracy of biochemical (^{1}H-MRSI) or functional (PET, f-MRI) data with anatomical (MRI, CT) data is in general difficult to assess for two main reasons. First, there is a large difference in the spatial resolution (~ 1 mm^3 for MRI, > 6 mm^3 for PET and ^{1}H-MRSI), necessitating the resampling of one modality along the planes of another in order to estimate the registration accuracy. Also, when dealing with clinical volumes, rarely is there an independent and clear measure of truth, unless an external fiducial system (such as a stereotactic frame) is included in both sets of scans.

Validation studies have been carried out for image modality registration algorithms, each with its own advantages and shortcomings. While the point-matching algorithm requires moderate expertise in anatomy and takes a few minutes, the actual computation time is negligible.[23] The accuracy of the landmark-registration method is inherently limited by the ability of the user to identify homologous points. Clearly the residual root-mean-square (rms) error decreases as the number of identified point pairs increases. In the registration of PET to MRI volumes a rms error of 0.5 mm was achieved when the rms inaccuracy in the identification of homologous points was 5 mm or less.[24] On the other hand, automated algorithms require little or no user intervention, but are generally computationally expensive. The accuracy of the automated algorithm used to register PET and MRI images has been shown to be < 2 mm^3.[22]

The method described for registering ^{1}H-MRSI to MRI described earlier relies on the critical assumption that the subject remained immobile between the targeting MRI scan and the following MRS imaging. A specialized MRI-to-MRI automated algorithm is used to register the global high-resolution MRI to the targeting MRI. As such, none of the features of the ^{1}H-MRSI are used in the registration process. Rather, the common features of the two MRI scans are used to find a transformation between the two spaces, and the same transformation is applied to the ^{1}H-MRSI to map it to the global MRI. Obviously if the subject did move and the above assumption is invalid, there will be a registration mismatch. Considering the spatial resolution of ^{1}H-MRSI, a slight mismatch may easily go unnoticed. However, careful visual inspection has shown that the ^{1}H-MRSI metabolite images match with structural images in the post processing stage. If the resolution of ^{1}H-MRSI were on the same order as the global MRI, such small registration errors would be more noticeable. However, because of the resolution difference between ^{1}H-MRSI and MRI, such errors are negligible.

https://doi.org/10.1017/S0317167100033436 Published online by Cambridge University Press

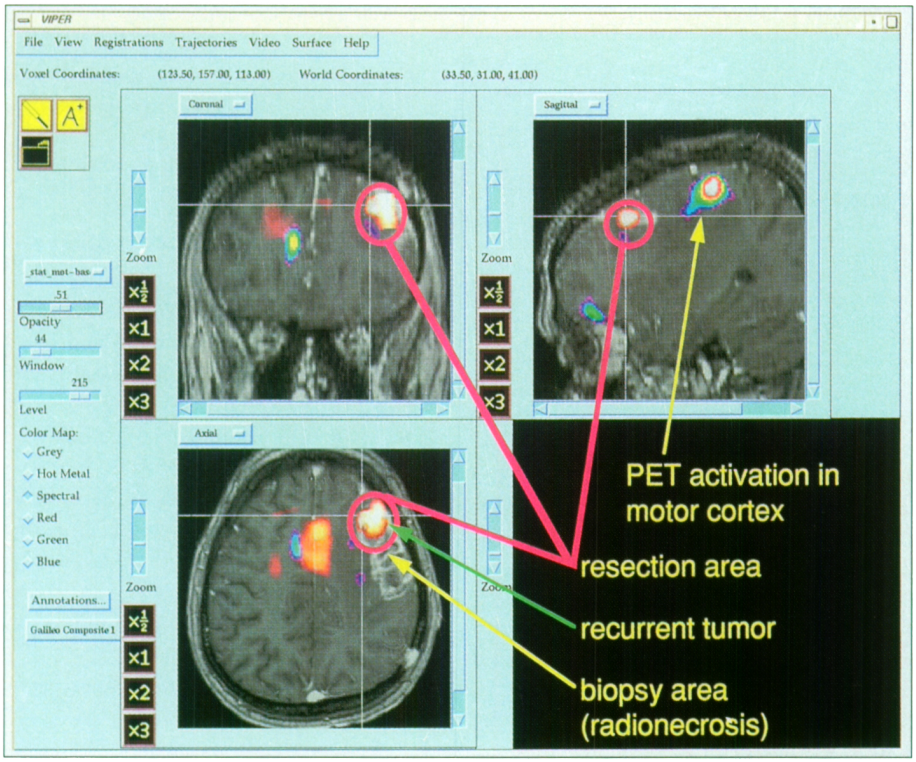

Figure 4: *The multimodal imaging integration of the Cho metabolite map, gadolinium-infused MRI, and f-PET as viewed on a screen display of the intraoperative, interactive, image-guided frameless stereotactic surgical navigation system. The triplanar view is situated at an optimum point at which to view the high Cho signal in coronal, transverse, and sagittal planes and also shows well the f-PET signal in the motor strip in the sagittal plane. Note that the area of resection encompassed the anterior region of high Cho signal. Biopsies were acquired along the posterior margin of the resection area. This integrated imaging scheme reveals that the area of high Cho signal is anterior and slightly inferior to the activated motor cortex seen on f-PET.*

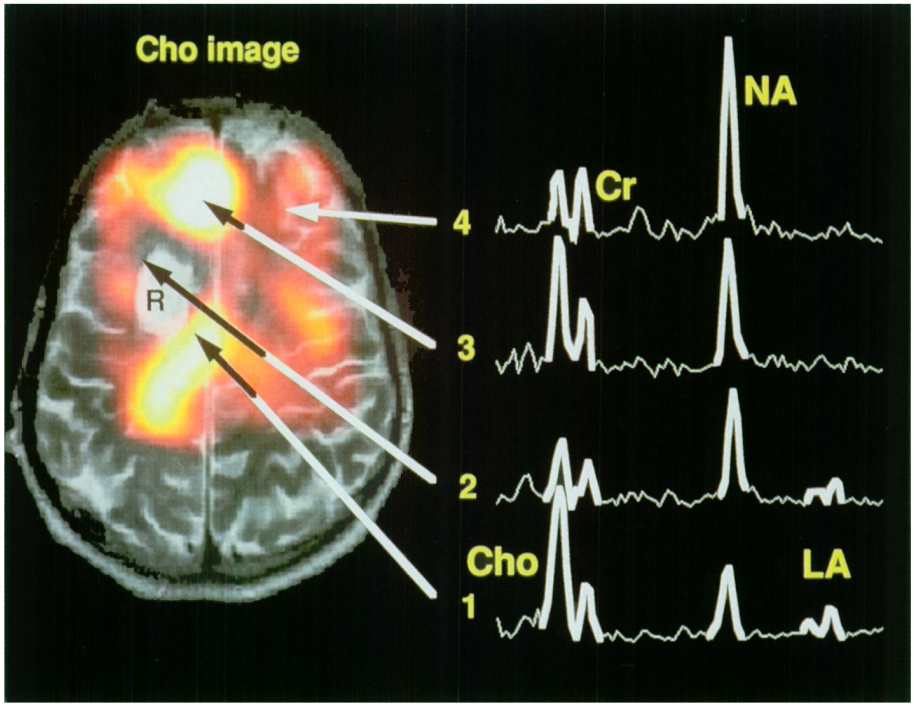

Figure 5: ***A)*** *Integrated Cho image with a corresponding transverse slice of the MRI indicates the locations of the recurrence of the oligodendroglioma and their relationship to the previous resection cavity (R). The area of high Cho signal anteriorly was included in the right frontal resection, while the posterior area of high Cho could not be resected because it involved the motor cortex. Spectra are shown along with the locations of their voxels. Note the high Cho peaks in spectra 1 and 3, and the LA peaks in spectra 1 and 2. (The relevant main metabolite peaks have been bolded for clarity.)*

https://doi.org/10.1017/S0317167100033436 Published online by Cambridge University Press

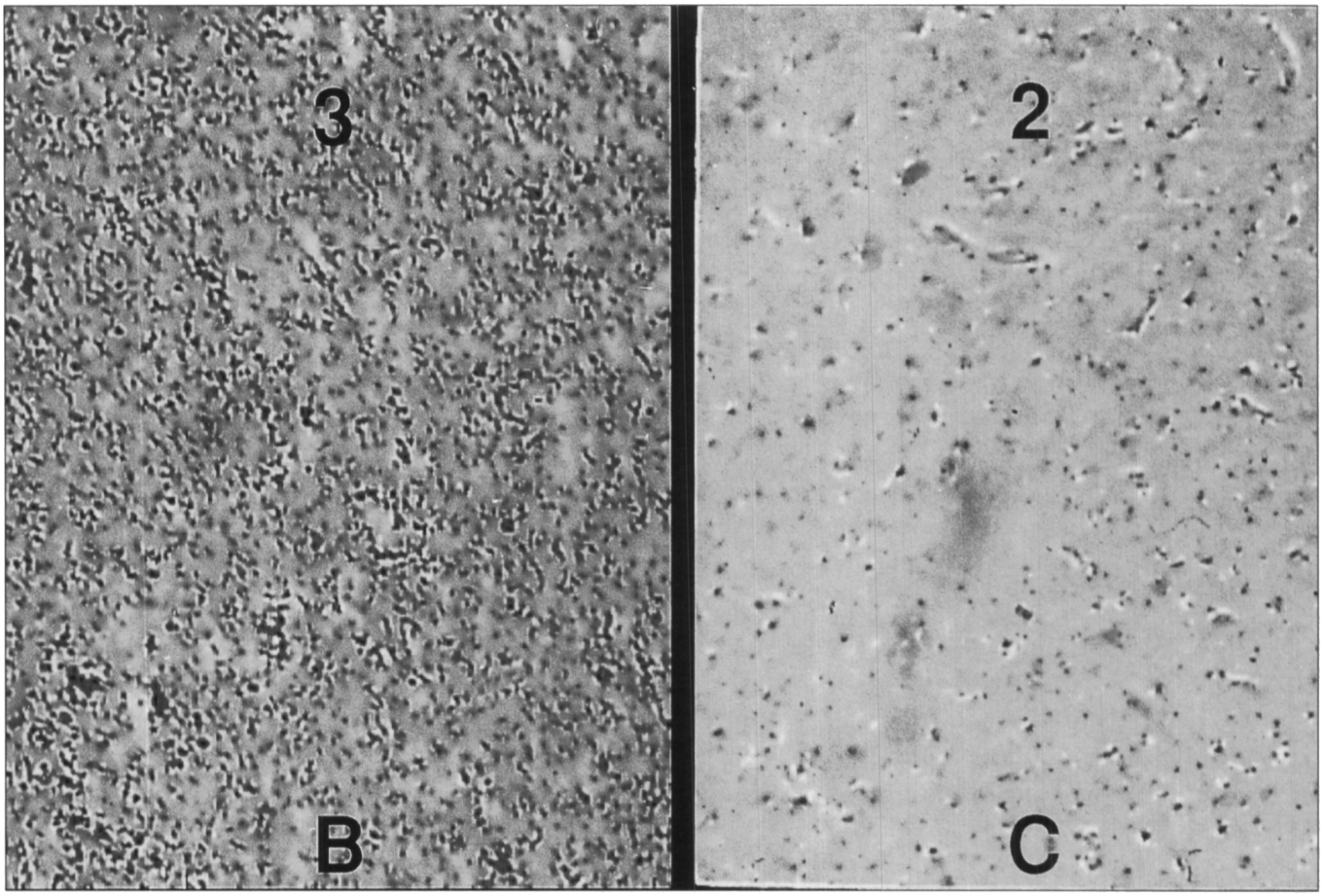

Figure 5: B) *While the tissue from spectrum 3 was composed of a grade II oligodendroglioma (spectra from this area showing high Cho and low NA), the biopsied tissue from the voxel of spectrum 1 showed oligodendroglioma with malignant changes (histological features suggested by spectra from the area displaying high Cho, low NA, and high LA).*[2-4] *The voxel corresponding to spectrum 2, which does not show high Cho signal, showed tissue* ***C)*** *consistent with post-radiation changes. Spectrum 2 also shows evidence of abnormal glycolysis as indicated by the LA peak. Spectrum 4 shows a normal pattern for human brain tissue. (Hematoxylin and eosin, 100x.)*

Discussion

Differentiation of Tumor Recurrence and Radiation Change

Despite advances in CT scanning and MRI technology, the differentiation between the recurrence of a glioma and radiation change, including necrosis, remains problematic and uncertain until histological confirmation is obtained. The differentiation of these two pathologies will become all the more important as treatment modalities presently under investigation, such as the use of agents that enhance the effects of radiotherapy (radiosensitizers) and genetic therapies which may be associated with an inflammatory response, come into wider use, if only in investigational protocols. We have demonstrated that ^{1}H-MRSI was able to differentiate dense regions of tumor recurrence from radiation effects in our two patients.

Nuclear medicine imaging, such as FDG PET and dual-isotope single-photon emission computed tomography (SPECT) may be useful in detecting regions of dense tumor growth in non-irradiated patients, but are relatively insensitive to less densely cellular regions and have so far not proved reliable in differentiating recurrent tumor from radiation necrosis.[6,7,25-29] With both modalities tumor can appear isointense with adjacent cortical grey matter complicating interpretation. Studies have indicated that FDG PET results cannot be correlated accurately with tumor progression in patients receiving intensive irradiation.[28,29] This lack of accuracy may be due to metabolic alterations in glucose metabolism of tumor cells exposed to radiation.[28] FDG PET is limited by availability, expensive cost, and lack of anatomical correlation for the metabolic data. In addition, for truly meaningful interpretation FDG PET must be acquired utilizing a more involved quantitative sequence.

Rapid MR imaging during bolus injection of contrast agent can generate maps of relative cerebral blood volume which may distinguish recurrent tumor that is highly vascularized from radionecrosis.[30] Differentiation of tumor from adjacent grey matter has, however, proven difficult. Such dynamic MR imaging would likely not have shown the areas of tumor recurrence in our second patient as the tumor did not show enhancement.

https://doi.org/10.1017/S0317167100033436 Published online by Cambridge University Press

Unlike FDG PET or SPECT which rely on radionuclide injection, ^{1}H-MRSI conveniently allows for the direct, noninvasive observation of multiple proton-containing metabolites simultaneously *in vivo*, either by quantification of spectral peaks or by reconstruction of images that show the regional distribution of the metabolites throughout a large region of interest. ^{1}H-MRSI sequences such as ours, or shorter sequences (although they may not yield high quality spectra, but are nonetheless quite usable) can be easily added to a conventional MR imaging examination and are well tolerated by most patients.

The elevated Cho pattern in these two patients with recurrent gliomas was similar to that observed in our experience with untreated gliomas.[1,2,31] We hypothesized that this pattern represented tumor recurrence. The increased signal from Cho seen in brain tumors is thought to reflect enhanced cellular membrane phospholipid synthesis accompanying tumor cell proliferation, increased cellularity, or increased amounts or mobility of choline-containing phospholipids within tumor cells.[5-7,18,32-34] Although not confirmed with biopsy at the time of ^{1}H-MRSI, two recent studies have shown increasing levels of Cho in tumors radiologically and clinically interpreted to be progressing;[6,7] and areas believed to be radionecrotic showed lowered Cho and inconsistently elevated levels of aliphatic resonances.[6] *In vitro* ^{1}H-MRSI analyses of surgically-removed astrocytoma specimens have generally indicated increases in Cho levels and decreases in NA levels – both of which have been shown to be associated with increases in tumor malignancy.[35-40] *In vivo* ^{1}H-MRSI studies of human astrocytomas have found a similar relationship between metabolic features and histopathological grade.[2,13,15,16,32,39,41-45] Furthermore, LA is more likely to be present in malignant tumors than in low-grade astrocytomas, and Lip is known to occur in tumors of higher histopathological grade.[2,35,46] Moreover, the presence of Lip in intact surgical specimens has been found to correlate with the amount of cellular necrosis seen under the microscope.[35,46]

Our first case showed low Cho and Cr, little, if any, NA and the presence of LA in the area preoperatively thought to be and histologically proved as radiation necrosis. In our second case histological examination did not show the massive necrotic changes that may be associated with irradiation, although moderate radiation effect changes, including vascular thickening and decreased cellularity, were present lateral to the previous resection margin. In this area, spectra showed decreased peaks for Cho, Cr, NA and low levels of LA. We and others have observed a pattern of significantly reduced MR metabolites in acellular regions and occasionally in the necrotic/cystic core of many malignant tumors or other lesions.[2-4,6] In these two patients the spectral pattern of significantly reduced metabolites with evidence of abnormal glycolysis (low levels of LA) in the areas histologically proven as showing changes due to irradiation effect was consistent with the type of tissue seen: relative acellularity, reactive astrocytes, vascular thickening, spotty areas of necrosis. Occasionally radiation changes may involve large areas of cystic necrosis similar to that seen in the cores of glioblastomas. In these cases, spectra would be expected to show large peaks for LA and Lip. Thus defining radiation change by means of a characteristic ^{1}H-MRSI spectrum may be difficult because of the range of changes that may be seen in irradiated brain tissue. In both of our cases, however, the Cho signal was low in the areas of radiation change, while it was high where recurrent tumor predominated. Thus, as evidenced by these two patients, the Cho signal may prove to be the most specific indicator for areas that are relatively dense in viable tumor cells. It may thus prove to be more expedient to define which locations harbor dense areas of recurrent tumor rather than where irradiation effected tissue predominates.

Histological examination of the tissue resected in our patients correlated to the corresponding ^{1}H-MRSI voxels confirms for the first time that regions with a high Cho signal in patients who have undergone post-operative irradiation correspond to areas where viable tumor predominates. These two cases suggest that it is possible to differentiate relatively dense areas of tumor recurrence from radiation effects by means of ^{1}H-MRSI. However when both conditions co-exist at the same location, it may be difficult to differentiate precisely where radiation effect ends and tumor begins. In this setting the boundaries distinguishing these two entities would need to be defined at the microscopic level, which is as yet beyond the capabilities of ^{1}H-MRSI.

Using ^{1}H-MRSI in an Integrated Multimodal Imaging System

The *in vivo* biochemical images obtained with ^{1}H-MRSI that show the regional heterogeneity of metabolite concentrations can be useful in surgical guidance,[3,4] allowing resection or biopsy of areas where maximal tumor activity is suspected. Multimodal image integration is becoming increasingly important for neurosurgical planning. Intraoperative, interactive, image-guided, frameless stereotactic systems have the potential to take advantage of the use of multimodal image integration not only for the identification of important deep brain structures or eloquent cortex, but also to display regional distributions of brain tumor metabolites indicating areas of tumor that differ in cellular composition. These cases show the advantage of the ^{1}H-MRSI data registered with other imaging data (such as routine MR sequences) or integrated smoothly into a multimodal image display system that affords localization of tissue specimens with corresponding voxels for spectral measurements. Further use of this system incorporating *in vivo* biochemical information will assess whether or not this system provides the surgeon with an improved ability to plan or guide the resection or biopsy of brain tumors.

Conclusions

We have demonstrated in two diagnostically difficult cases that the differentiation between relatively dense areas of tumor recurrence and radiation change may be achieved using ^{1}H-MRSI in patients whose neurodiagnostic interpretation based on CT or MRI is equivocal for such a differentiation. We are currently in the process of expanding our experience using ^{1}H-MRSI for the localization of recurrent tumor. Integrated with conventional MRI, ^{1}H-MRSI can guide the extent of resection, limiting it to the area of tumor recurrence, thus avoiding damage to eloquent regions that grossly and radiologically may appear just as abnormal as the area of tumor infiltration. As such the usefulness of ^{1}H-MRSI in brain tumor patients extends beyond simple diagnosis of tumor type and enters the realm of therapeutic guidance. The surgical utility of metabolic images from ^{1}H-MRSI can be further enhanced by co-registration with data sets from other imaging modalities into a frameless stereotactic, image-guided surgical navigation system.

https://doi.org/10.1017/S0317167100033436 Published online by Cambridge University Press

REFERENCES

1. Preul MC, Collins DL, Arnold DL. Differential diagnosis of human intracranial tumors *in vivo* using 1H-MR spectroscopic imaging and feature space for spectral pattern recognition. *In*: Shorvon SD, Fish DR, Andermann F, Bydder GM, Stefan H, eds. Magnetic Resonance Scanning and Epilepsy. New York: Plenum, 1993: 299-313.
2. Preul MC, Caramanos Z, Collins DL, et al. Accurate, noninvasive diagnosis of human brain tumors by using proton magnetic resonance spectroscopy. Nature Medicine 1996; 2: 323-325.
3. Preul MC, Narayanan S, Comeau R, et al. Intraoperative, interactive guidance of stereotactic brain tumor biopsy or resection using *in vivo* biochemical image - anatomical image integration. J Neurosurg 1996; 84: 344A.
4. Preul MC, Caramanos Z, Leblanc R, et al. Improved stereotactic brain tumor biopsy or resection using *in vivo* biochemical imaging: accurate prediction of regional tissue chemicopathological characteristics leads to more accurate target planning. J Neurosurg 1997; 86: 361A-362A.
5. Heesters MA, Kamman RL, Mooyaart EL, Go KG. Localized proton spectroscopy of inoperable brain gliomas. Response to radiation therapy. J Neurooncol 1993; 17: 27-35.
6. Wald LL, Nelson SJ, Day MR, et al. Serial proton magnetic resonance spectroscopy imaging of glioblastoma multiforme after brachytherapy. Journal of Neurosurgery 1997; 87: 525-534.
7. Tedeschi G, Lundbom N, Raman R, et al. Increased choline signal coinciding with malignant degeneration of cerebral gliomas: a serial proton magnetic resonance spectroscopy imaging study. Journal of Neurosurgery 1997; 87: 516-524.
8. Culver KW, Rom Z, Wallbridge S, et al. *In vivo* gene transfer with retroviral-producer cells for the treatment of experimental brain tumors. Science 1992; 256: 1550-1552.
9. Moolten FL, Wells JM. Curability of tumors bearing herpes thymidine kinase genes transferred by retroviral vectors. Journal of the National Cancer Institute 1990; 82: 297-300.
10. Ezzedine ZD, Martuza RL, Platika D, et al. Selective killing of glioma cells in culture and *in vivo* by retrovirus transfer of the herpes simplex thymidine kinase gene. New Biologist 1991; 3: 608-614.
11. Ram Z, Culver KW, Walbridge S, Blaese RM, Oldfield EH. *In situ* retroviral-mediated gene transfer for the treatment of brain tumors in rats. Cancer Research 1993; 53: 83-88.
12. Sandoz Pharma Ltd. Study no. GLIB 201-E-00 Gene therapy for the treatment of glioblastoma multiforme with *in vivo* tumor transduction with the herpes simplex thymidine kinase gene/ganciclovir system. Sandoz Pharma Ltd 1995.
13. Fulham MJ, Bizzi A, Dietz MJ, et al. Mapping of brain tumor metabolites with proton MR spectroscopic imaging: clinical relevance. Radiology 1992; 185: 675-686.
14. Furuya S, Naruse S, Ide M, et al. [The clinical application of multivoxel 1H-CSI (chemical shift imaging) in brain tumors]. [Japanese]. Nippon Igaku Hoshasen Gakkai Zasshi 1991; 51: 836-838.
15. Alger JR, Frank JA, Bizzi A, et al. Metabolism of human gliomas: assessment with H-1 MR spectroscopy and F-18 fluorodeoxyglucose PET [see comments]. Radiology 1990; 177: 633-641.
16. Negendank WG, Sauter R, Brown TR, et al. Proton magnetic resonance spectroscopy in patients with glial tumors: a multicenter study. J Neurosurg 1996; 84: 449-458.
17. Kauppinen RA, Williams SR. Nuclear magnetic resonance spectroscopy studies of the brain. [Review]. Prog Neurobiol 1994; 44: 87-118.
18. Klein J, Koppen A, Loffelhoz K, Schmitthenner J. Uptake and metabolism of choline by rat brain after acute choline administration. Journal of Neurochemistry 1992; 58: 870-876.
19. Sibson R. Studies in the robustness of multidimensional scaling: Procrustes statistics. Journal of the Royal Statistical Society 1978; 40: 234-238.
20. Collingnon A, Maes F, Delaere D, et al. Automated muli-modality image registration based on information theory. Information Processing in Medical Imaging 1995; proceedings: 263-274.
21. Collins DL, Neelin P, Peters TM, Evans AC. Automatic 3-D intersubject registration of MR volumetric data in standardized Talairach space. Journal of Computer Assisted Tomography 1994; 18: 192-205.
22. Woods RP, Mazziotta JC, Cherry SR. MRI-PET registration with automated algorithm. J Comput Assist Tomogr 1993; 17: 536-546.
23. Neelin P, Crossman J, Hawkes DJ, Ma Y, Evans AC. Validation of an MRI/PET landmark registration method using 3D simulated PET images and point simulations. Computerized Medical Imaging and Graphics 1993; 17: 351-356.
24. Evans AC, Marrett S, Torrescorzo J, Ku S, Collins DL. MRI-PET correlation in three dimensions using a volume of interest (VOI) atlas. Journal of Cerebral Blood Flow and Metabolism 1991; 11: A69-A78.
25. Alexander E3rd, Loeffler JS, Schwartz RB, et al. Thallium-210 technetium-99m HMPAO single-photon emission computed tomography (SPECT) imaging for guiding stereotactic craniotomies in heavily irradiated mailgnant glioma patients. Acta Neurochirurgica (Wien) 1993; 122: 215-217.
26. Buchpiguel CA, Alavi JB, Alavi A, Kenyon LC. PET versus SPECT in distinguishing radiation necrosis from tumor recurrence in the brain [clinical conference]. Journal of Nuclear Medicine 1995; 36: 159-164.
27. Schwartz RB, Carvalho PA, Alexander E3rd, et al. Radiation necrosis vs. high-grade recurrent glioma: differentiation by using dual-isotope SPECT with 201TI and 99mTc-HMPAO. American Journal of Neuroradiology 1991; 12: 1187-1192.
28. Tyler JL, Villemure JG, Evans AC, et al. Metabolic and hemodynamic evaluation of gliomas using positron emission tomography. Journal of Nuclear Medicine 1987; 28: 1123-1133.
29. Janus TJ, Kim EE, Tilbury R., et al. Use of [18F]fluorodeoxyglucose positron emission tomography in patients with primary malignant brain tumors. Annals of Neurology 1993; 33: 540-548.
30. Aronen HJ, Gazit IE, Louis DN, et al. Cerebral blood volume maps of gliomas: comparison with tumor grade and histologic findings. RAdiology 1994; 191: 41-51.
31. Preul MC, Caramanos Z, Collins DL, Arnold DL. Linear discriminant analysis based on proton MR spectroscopic imaging of human brain tumors improves pre-operative diagnosis. Proc Soc Magn Reson 1994; 2: 125 (Abstract).
32. Luyten PR, Marien AJH, Heindel W, et al. Metabolic imaging of patients with intracranial tumors 1H MR spectroscopic imaging and PET. RAdiology 1990; 176: 791-799.
33. Cristensen H, Lour HO, Clausen J, Biering F. Phospholipids and glycolipids of tumors of the central nervous system. Journal of Neurochemistry 1965; 12: 614-627.
34. Miller BL, Chang L, Booth R. *In vivo* 1H-MRS choline: correlation with *in vitro* chemistry/histology. Life Sciences 1996; 58: 1929-1935.
35. Kuesel AC, Donnelly SM, Halliday W, Sutherland GR, Smith IC. Mobile lipids and metabolic heterogeneity of brain tumors as detectable by *ex vivo* 1H MR spectroscopy. NMR Biomed 1994; 7: 172-180.
36. Usenius JP, Kauppinen RA, Vainio PA, et al. Quantitative metabolite patterns of human brain tumors: detection by 1H NMR spectroscopy *in vivo* and *in vitro*. J Comput Assist Tomogr 1994; 18: 705-713.
37. Remy C, Arus C, Ziegler A, et al. *In vivo*, *ex vivo*, and *in vitro* one- and two-dimensional nuclear magnetic resonance spectroscopy of an intracerebral glioma in rat brain: assignment of resonances. J Neurochem 1994; 62: 166-179.
38. Peeling J, Sutherland G. High-resolution 1H NMR spectroscopy studies of extracts of human cerebral neoplasms. Magn Reson Med 1992; 24: 123-136.

39. Gill SS, Thomas DG, Van Bruggen N, et al. Proton MR spectroscopy of intracranial tumors: *in vivo* and *in vitro* studies. J Comput Assist Tomogr 1990; 14: 497-504.
40. Steen RG. Response of solid tumors to chemotherapy monitored by *in vivo* 31P nuclear magnetic resonance spectroscopy: a review. Cancer Research 1989; 49: 4075-4085.
41. Demaerel P, Johannik K, Van Hecke P, et al. Localized 1H NMR spectroscopy in fifty cases of newly diagnosed intracranial tumors. J Comput Assist Tomogr 1991; 15: 67-76.
42. Arnold DL, Shoubridge EA, Villemure JG, Feindel W. Proton and phosphorus magnetic resonance spectroscopy of human astrocytomas *in vivo*. Preliminary observations on tumor grading. NMR Biomed 1990; 3: 184-189.
43. Segebarth CM, Baleriaux DF, Luyten PR, den Hollander JA. Detection of metabolic heterogeneity of human intracranial tumors *in vivo* by 1H NMR spectroscopic imaging. Magn Reson Med 1990; 13: 62-76.
44. Bruhn H, Frahm J, Gyngell ML, et al. Noninvasive differentiation of tumors with use of localized H-1 MR spectroscopy *in vivo*: initial experience in patients with cerebral tumors [see comments]. Radiology 1989; 172: 541-548.
45. Usenius JP, Tuohimetsa S, Vainio P, et al. Automated classification of human brain tumors by neural network analysis using *in vivo* 1H magnetic resonance spectroscopic metabolite phenotypes. Neuroreport 1996; 7: 1597-1600.
46. Kuesel AC, Sutherland GR, Halliday W, Smith IC. 1H MRS of high grade astrocytomas: mobile lipid accumulation in necrotic tissue. NMR Biomed 1994; 7: 149-155.